NUMERICAL INVESTIGATION OF NONLINEAR DIFFRACTION WAVE LOADS ON A SUSPENDED CYLINDER

Ming Wang 1
Department of Civil and Environmental Engineering, UPC-BarcelonaTech
e-mail: wang.ming@upc.edu

Anna Mujal-Colilles 2
Department of Nautical Studies and Engineering, UPC-BarcelonaTech
e-mail: anna.mujal@upc.edu

CLIMENT MOLINS 3
Department of Civil and Environmental Engineering, UPC-BarcelonaTech
e-mail: climent.molins@upc.edu

Abstract

Floating offshore wind turbines (FOWTs) interact with waves in complex sea conditions, in particular wave-induced nonlinear diffraction wave loads can excite the resonant response of FOWTs in the low frequency range. In this paper, a fixed rigid suspended cylinder (considered a simplification of the support columns of a complex structure) is analyzed for nonlinear wave loads under regular waves using OpenFOAM, an open-source Computational fluid dynamics (CFD) software. Meanwhile, the default shallow water wave absorption boundary is optimized for deep water to enable the simulation of FOWTs in a real environment. Finally, results are compared with experimental and potential flow analysis with the CFD model yielding better estimates of first, second and third order wave diffraction loads than the engineering model using potential flow theory. Engineering models based on second-order potential flow theory are not effective in predicting the second and third order wave diffraction loads.

Keywords: Suspended cylinder; CFD; OpenFOAM; Nonlinear diffraction wave loads

1. INTRODUCTION

Recently, Floating Offshore Wind Turbines (FOWTs), using floating platforms, have been successful in overcoming the visual and environmental pollution (Jonkman, 2007) caused by traditional near-shore wind turbines because they can be installed in deep water areas away from the shoreline. Meanwhile, wind resources are more abundant in areas far from the shoreline than in nearshore areas(Archer & Jacobson, 2005), and FOWTs are cheaper to build than bottom-fixed OWTs in deep waters (Jonkman, 2007). However, there are two sides to the coin, and while FOWTs offer the above advantages, it also presents several important challenges. With increasing water depth, the harsh environment and steep waves can lead to highly nonlinear wave hydrodynamic loads on the floaters of FOWTs. Also, high frequency loads can cause springing and ringing, and low frequency loads can cause sway and yaw of the moored platform. Therefore, how to accurately predict the nonlinear hydrodynamic loads on FOWTs is the focus of current research.

Many studies (Goupee et al., 2013; Duan et al., 2016; Viselli et al., 2015) have been conducted to predict the dynamic response of FOWTs under different conditions by carrying out scaling experiments of various

sizes. However, model experiments are expensive, difficult to operate for larger sizes, and the model experiments cannot satisfy both the Froude scaling law and the Reynolds similarity law. Numerical methods are widely used because it overcomes the shortcomings of experimental tests. In the engineering field, potential flow theory is usually combined with a Morison-type viscous drag model to predict the hydrodynamic loads of various FOWTs (Li & Bachynski-Polić, 2021). On the other hand, Benitz et al. (2014) demonstrated that computational fluid dynamics (CFD) has the ability to more accurately predict nonlinear difference frequency wave loads and capture oscillatory loads caused by vortex shedding.

The complexity of cyclic boundary conditions applied to numerical methods has been reduced after Higuera et al. (2013) developed a wave generation and Active Wave Absorption (AWA) that does not require additional computational domains for traditional damping zone. Active Wave Absorption (AWA) offset the effects caused by reflected waves by adding a velocity to the boundary that is opposite to the direction of the reflected waves.

This study presents the results obtained using CFD of the experiment carried on a suspended rigid cylinder can be considered as a simplification of the support columns of a complex platform. The experimental case used is first presented and the parameters of the numerical model are introduced in Section 2. In addition, the mesh convergence and the improved active wave absorption boundary are verified. In Section 3, results such as the wave and surge forces are analyzed in the time and frequency domains, respectively, and compared with potential flow results. The conclusions are provided in Section 4.

2.   CASE OF STUDY

2.1   Case of study

In the present work, to investigate nonlinear hydrodynamic loads on a rigid cylinder in a regular wave, full-scale experiments (Marthinsen et al., 1996; Stansberg et al., 1995; Vugts & Technische Universiteit Delft., 1997) at MARINTEK in Trondheim, Norway, were selected and compared with potential flow theory results using the Stokes 2nd order wave model in Case 9 of the experiments (Robertson et al., 2015). A suspended cylinder is fixed by a rigid frame and placed at the center of the tank length (38.6 m) and width (5.25 m) and the depth of the tank is 10 m, as shown in Fig.1. The cylinder draft is 1.44 m. The characteristic frequency of the structure is greater than $10\ Hz$ with the rigid frame. The regular wave in Case 9 is a deep-water wave with a wave height of 0.282 m and a period of 2.114 s. To be consistent with the experimental setup, a right-handed coordinate system was chosen for this study. The positive direction of coordinate axis x is the direction of wave flow, and the direction of z is vertically upward.
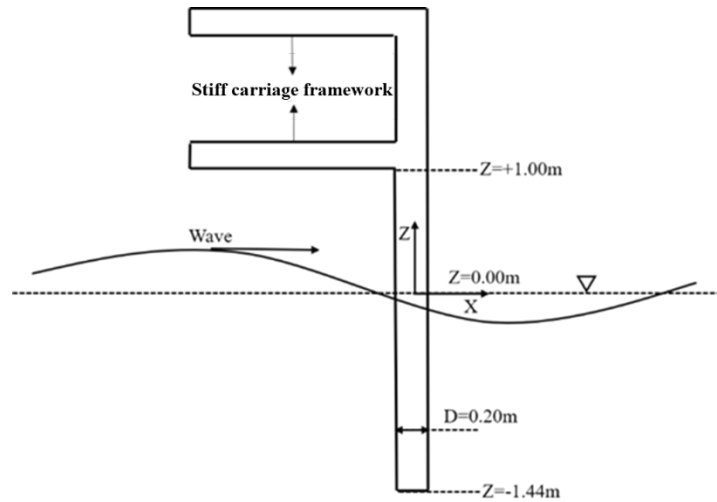
Fig. 1 Schematic representation (not to scale) of the case setup for a fixed vertical cylinder encountering incoming waves.

2.2 Numerical model

OpenFOAM is a leading open-source software for Computational fluid dynamics (CFD) that is widely used in industry and scientific community. In this paper, we adopt the interFoam solver in OpenFOAM, which is a fully nonlinear Navier-Stokes solver. Complex free surface flow and fluid-solid interaction are simulated using the VOF method. IHFoam, as an extension of interFoam, adds wave generation and absorption developed by Higuera et al. (2013) to interFoam. This method of wave absorption can reduce the computational resources by more than 30% (Vyzikas et al., 2018).
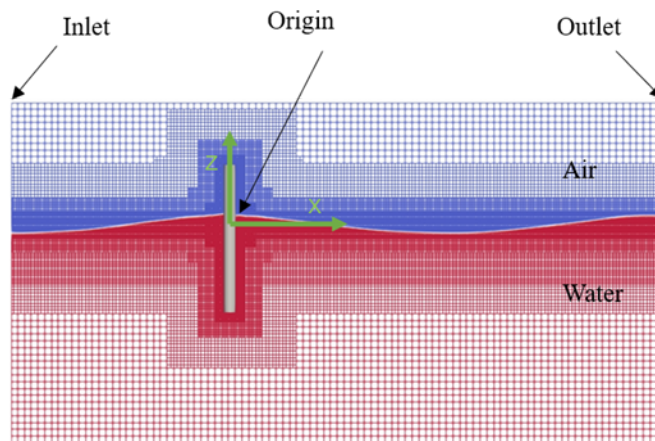
Fig. 2   The computational field and mesh around suspended cylinder in the CFD simulations.

In order to reduce the computational time. As shown in Fig. 2, a half domain was adopted in this study. The right-hand coordinate system starts from the center of the water plane of the suspended cylinder, the wave flow direction is the positive direction of x, and the opposite direction of gravity is the positive direction of z. The length of the numerical computational domain is 10.8 m, the height is 5.6 m, and the water depth is 3.6 m

(deep water wave condition). In addition, the height of the air domain is 2 m. The numerical computational domain does not use the settings of the experimental basin. This is because the following boundary reflection tests show that even using the current settings of the computational domain, Active Wave Absorption (AWA) is sufficient to eliminate the reflected waves. Waves are simulated using Stokes 5th order waves. The mesh is fixed and generated unstructured mesh by Star CCM+. The size of each background mesh is 0.112 m in all directions. Thereafter, the mesh was refined for the free surface and cylinder surface. In order to determine the size of the refinement mesh, a mesh convergence study was performed for the free surface elevation, using four different mesh sizes and a laminar flow model was chosen in order to avoid the influence of the turbulence model. In Table. 1, the wave heights obtained from the four different meshes are compared. The results of the finest grid are used as a baseline.

Fig. 3 shows that the free surface elevation difference gradually decreases with the mesh size. The difference in free surface elevation between H/20 (H is wave height) and H/40 is only 0.3%, and the accuracy of the H/20 mesh is considered accurate enough for the current study and will be used for subsequent simulation. For the turbulence model, 5 cell layers adjacent to the cylinder surface are generated. The thickness of the first layer is 5.0 mm and its expansion ratio is 1. The simulation lasts for 30 cycles and the last 20 cycles are taken for data. As Devolder et al. (2018) describes, wave simulations sometimes produce excessive wave damping when Reynolds-Averaged Navier-Stokes (RANS) performs turbulence modeling using the K-Omega SST turbulence model. Such anomalies can be prevented by adding a buoyancy term to the turbulence model. Therefore, buoyancy-modified K-Omega SST turbulence model (Devolder et al., 2017) was chosen for the current work.

Table. 1 Mesh convergence study. Errors in the wave height is computed with reference to the H/40 results.

Spatial discretization	Calculated wave height at origin (m)	Error	Calculation time for one wave cycle (i7-10700 with 8 cores)
H/5	0.2340	7%	72s
H/10	0.2445	2.83%	569s
H/20	0.2506	0.39%	4048s
H/40	0.2516	0	7477s
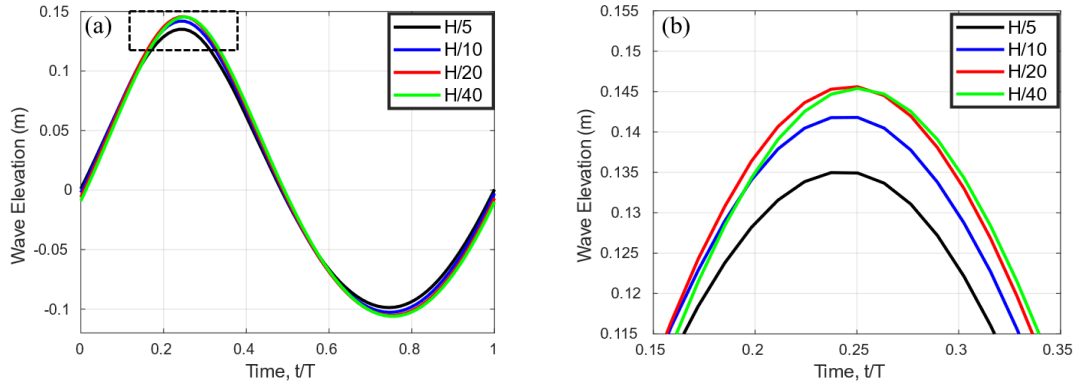
Fig. 3   Comparison of surface elevations of different meshes with no cylinder present. a) full wave elevation domain –dashed rectangle indicates the zoom-in of Fig 3b, b) zoomed-in view of wave peaks in the dashed box of Fig. 3a.

Since the default wave absorption boundary of IHFoam is using the shallow water theory, it is not applicable to the deep-water conditions studied in this paper. Higuera (2020) extends the velocity correction equation for arbitrary water depth conditions. The velocity correction equation for arbitrary water depth is as follows:

$$\Delta U = -\Delta \eta \omega \frac{\cosh \cosh [k(h+z)]}{\sinh \sinh [kh]} \#(1)$$

where ΔU is the velocity correction, h is the water depth, $\Delta \eta$ is the difference in free surface elevation due to the reflected wave.

To verify the validity of the new deep water wave absorption boundary condition, reflection analysis was performed for two of the periods in the simulation using WAVELAB software. Fig. 4 left shows the free surface elevation time series of incident and reflected waves for the new wave absorption boundary condition, where the reflected wave height is only 10% of the incident wave height. Two peaks can be seen on the right of Fig. 4 corresponding to the main harmonic (f=1/T) and the double frequency superharmonic (f=2/T). The absorption of the two frequency waves satisfies the subsequent study, but the reflected energy of the second superharmonic is significantly larger than that of the main harmonic.
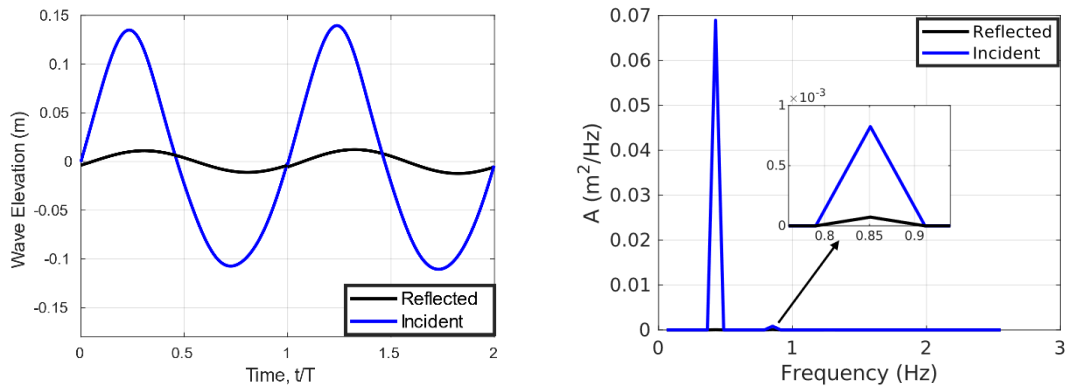
Fig. 4   Analysis of incident and reflected waves. Left: Time domain analysis. Right: Amplitude spectrum analysis.

3.   RESULTS

3.1   Free surface elevation

Fig. 5 shows the wave elevation time history for five periods. In general, CFD is in good agreement with the potential flow theory and experimental results. However, the trough of CFD is smaller and flat than the results of the other two methods. This is due to the wave trough being too close to the boundary of the mesh refinement area in the numerical domain.
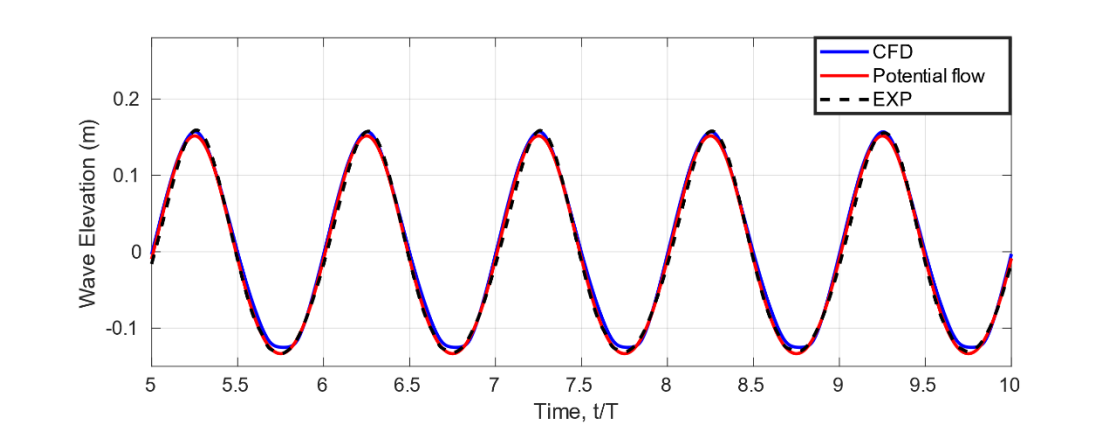
Fig. 5   Comparison of wave elevation time history (without structure participation).
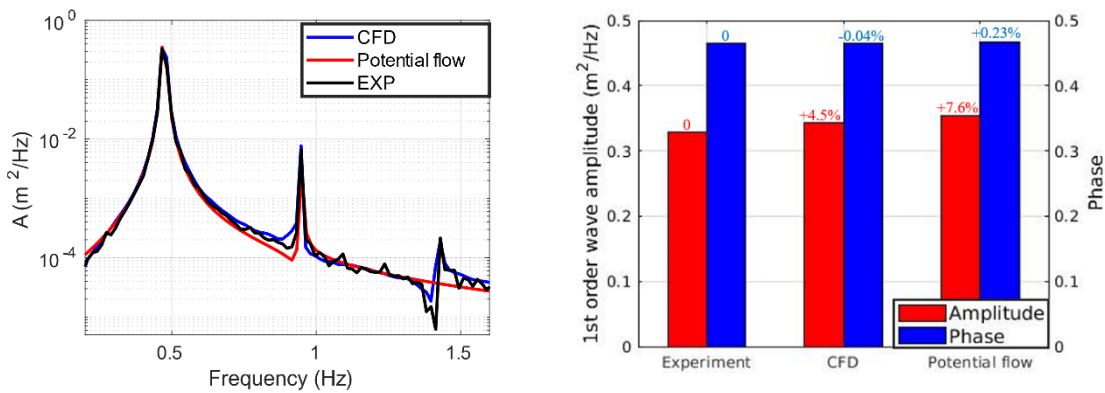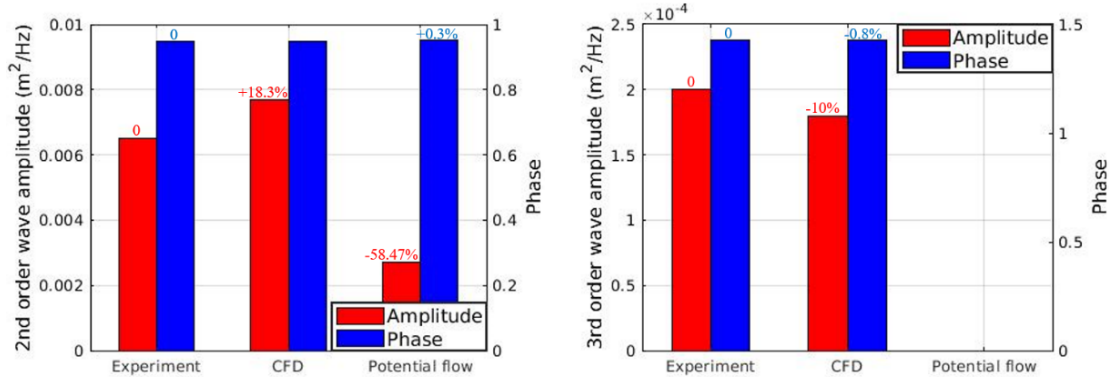
Fig. 6 Comparison of CFD, experimental and potential flow theory for PSD of wave elevation. Top left: the first three peaks of the wave elevation. Top right: first harmonic amplitude. Bottom left: second harmonic amplitude. Bottom right: third harmonic amplitude. The percentage on top of each bar represents the difference compared to the experimental results.

The PSD results of wave elevation for CFD and the other two methods are shown in Figure 6. The first three order harmonic amplitudes of the CFD results are consistent with the experimental results both in terms of trend and peak (magnitude and frequency) as can be seen on the top left of Fig. 6. The potential flow theory results failed to capture the second and third order harmonic amplitudes correctly compared to the CFD and experimental results. From the top right of Fig. 6, the results of the three methods differ little for the first order harmonic amplitude component. The main difference is in the amplitude (CFD: +4.5%, potential flow: +7.6%).

3.2 Surge forces

The time history of the surge force of the cylinder is shown in Fig. 7 and the peaks of the three methods are in good agreement. The troughs of the CFD results are larger compared with the experimental values but the trend is the same, while the troughs of the potential flow theory results are slightly different from the experimental values both in value and trend.

Fig. 8 shows the PSD of the surge force. From the top left of Fig. 8, the CFD method successfully captures the third-order peak and combined with the bottom right of Fig. 8, the CFD results agree well with the experimental results (error: -2.6%). This third peak has been shown to be related to the ringing of the structure, so even if it is small, it is still important (Vugts & Technische Universiteit Delft., 1997). The potential flow theory PSD results for the surge force are similar to the wave amplitude results in that they are only consistent with the experimental values in terms of phase, but cannot effectively capture the higher order components.
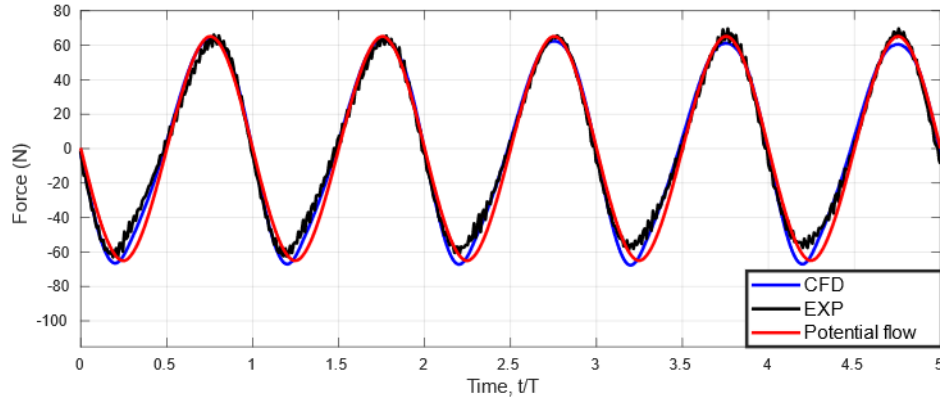
Fig. 7   Comparisons of surge force (CFD, Experiment and Potential flow).
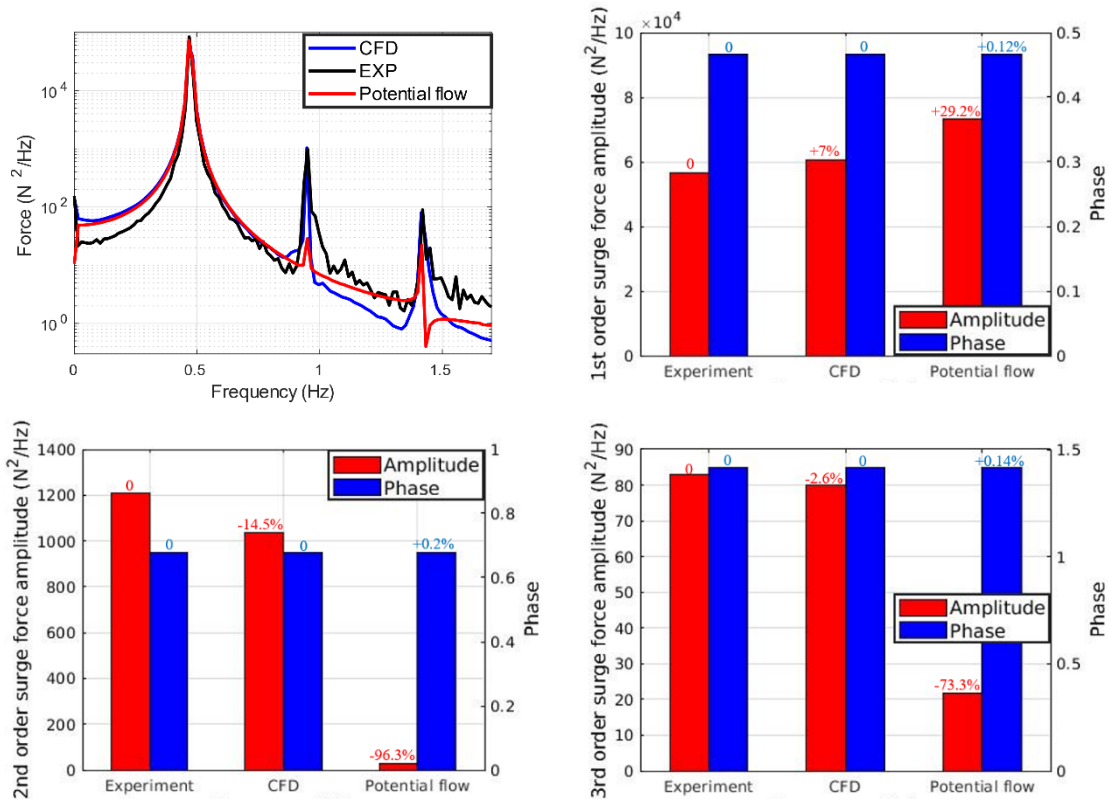
Fig. 8   Comparison of CFD, experimental and potential flow theory for PSD of horizontal hydrodynamics. Top left: the first three peaks of the horizontal hydrodynamics. Top right: first harmonic force. Bottom left: second harmonic force. Bottom right: third harmonic force. The percentage on top of each bar represents the difference compared to the experimental results.

4.   CONCLUSIONS

Active Wave Absorption (AWA) can effectively reduce the wave reflection at the outlet boundary so that the size of the computational domain can be greatly reduced. However, the present work has only investigated a

simple cylinder and a single wave. It is not confirmed whether AWA is effective for different waves and complex structures, so further tests are needed. Nonlinear wave loads, especially the third-order harmonic force components, are important for the design of FOWTs. In this paper, the accuracy of both CFD and potential flow theory methods are investigated by comparing experimental measurements of simple structures using both methods. In general, both CFD method and potential flow theory can obtain the correct phase but potential flow theory based on low order wave model cannot obtain the higher order components correctly. The CFD method can predict the higher-order components relatively accurately, but the CFD method still underestimates the second-order harmonic force components by 14.5%. This may be related to the fact that the second-order harmonic force is reflected by the boundary (the second-order amplitude reflection is significantly larger than the first-order amplitude reflection in subsection 1.2).

5.   REFERENCES

Archer, C. L.; Jacobson, M. Z. Evaluation of global wind power. *Journal of Geophysical Research D: Atmospheres* [online]. American Geophysical Union, 2005, vol. 110, no. D12, p. 1–20. eISSN 2169-8996. [Accessed: June 2022]. Available at: <https://doi.org/10.1029/2004JD005462>.

Benitz, M. A.; Schmidt, D. P.; Lackner, M. A.; Stewart, G. M.; Jonkman, J.; Robertson, A. Comparison of Hydrodynamic Load Predictions Between Reduced Order Engineering Models and Computational Fluid Dynamics for the OC4-DeepCwind Semi-Submersible. In: *Proceedings of the International Conference on Offshore Mechanics and Arctic Engineering - OMAE*, *9B* [online]. ASME, 2014. Available at: <https://doi.org/10.1115/OMAE2014-23985>

Devolder, B.; Rauwoens, P.; Troch, P. Application of a buoyancy-modified k-ω SST turbulence model to simulate wave run-up around a monopile subjected to regular waves using OpenFOAM®. *Coastal Engineering* [online]. 2017, vol. 125, p. 81–94. eISSN 0378-3839. [Accessed: June 2022]. Available at: <https://doi.org/10.1016/J.COASTALENG.2017.04.004>.

Devolder, B.; Troch, P.; Rauwoens, P. Performance of a buoyancy-modified k-ω and k-ω SST turbulence model for simulating wave breaking under regular waves using OpenFOAM®. *Coastal Engineering* [online]. Elsevier, 2018, vol. 138, p. 49–65. eISSN 0378-3839. [Accessed: June 2022]. Available at: <https://doi.org/10.1016/J.COASTALENG.2018.04.011>.

Duan, F.; Hu, Z.; Niedzwecki, J. M. Model test investigation of a spar floating wind turbine. *Marine Structures*, Elsevier, 2016, vol. 49, p. 76–96. eISSN 0951-8339. [Accessed: June 2022]. Available at: <https://doi.org/10.1016/J.MARSTRUC.2016.05.011>.

Goupee, A.; Robertson, A.; Coulling, A. J.; Goupee, A. J.; Robertson, A. N.; Jonkman, J. M.; Dagher, H. J. Validation of a FAST semi-submersible floating wind turbine numerical model with DeepCwind test data. *The Journal of Renewable and Sustainable Energy* [online]. AIP Publishing, 2013,vol. 5, no. 2, p. 10.1063/1.4796197. eISSN 1941-7012**.** [Accessed: June 2022]. Available at: <https://doi.org/10.1063/1.4796197>.

Higuera, P. Enhancing active wave absorption in RANS models. *Applied Ocean Research* [online]. Elsevier, 2020, vol. 94, no. 102000. eISSN 0141-1187. [Accessed: June 2022]. Available at: <https://doi.org/10.1016/J.APOR.2019.102000>.

Higuera, P.; Lara, J. L;, Losada, I. J. Realistic wave generation and active wave absorption for Navier–Stokes models: Application to OpenFOAM®. *Coastal Engineering* [online]. 2013, vol. 71, p. 102–118. eISSN 0378-3839. [Accessed: June 2022]. Available at: <https://doi.org/10.1016/J.COASTALENG.2012.07.002>.

Jonkman, J. *Dynamics modeling and loads analysis of an offshore floating wind turbine* [online]. Doctoral thesis. Colorado State University. Department of Aerospace Engineering Sciences, 2007. [Accessed: June 2022]. Available at: <https://search.proquest.com/openview/39165bc16cdf6381cd2c9814d06afdb7/1?pq-origsite=gscholar&cbl=18750>.

Li, H.; Bachynski-Polić, E. E. Validation and application of nonlinear hydrodynamics from CFD in an engineering model of a semi-submersible floating wind turbine. *Marine Structures* [online]. Elsevier,

2021, vol. 79, no. 103054. eISSN 0951-8339. [Accessed: June 2022]. Available at: <https://doi.org/10.1016/J.MARSTRUC.2021.103054>.

Marthinsen, T.; Stansberg, C. T.; Krokstad, J. R. . On the ringing excitation of circular cylinders. In: *The Sixth International Offshore and Polar Engineering Conference (ISOPE 1996): Los Angeles, California, USA, May 26-31, 1996* [online]. ISOPE: OnePetro, 1996. No. ISOPE-I-96-030. [Accessed: June 2022]. Available from:<https://onepetro.org/ISOPEIOPEC/proceedings-abstract/ISOPE96/All-ISOPE96/ISOPE-I-96-030 /23337>.

Robertson, A. N.; Wendt, F. F.; Jonkman, J. M.; Popko, W.; Vorpahl, F.; Stansberg, C. T.; Bachynski, E. E.; Bayati, I.; Beyer, F.; de Vaal, J. B.; Harries, R.; Yamaguchi, A.; Shin, H.; Kim, B.; van der Zee, T.; Bozonnet, P; Aguilo, B;, Bergua, E.;, Qvist, J.[et al.]. OC5 Project phase I: validation of hydrodynamic loading on a fixed cylinder. In: *International Offshore and Polar Engineering Conference (ISOPE 2015): Kona, Hawaii, USA,, June 21–26, 2015* [online]. NREL:, OnePetro, 2015. No. NREL/CP-5000-63567. [Accessed: June 2022]. Available at: <https://a2e.energy.gov/data/oc5/oc5.phase1a/attach/robertson-oc5-phase-ia.pdf>.

Stansberg, C. T.; Huse, E;, Krokstad, J. R.; Lehn, E. Experimental study of non-linear loads on vertical cylinders in steep random waves. In: *The Fifth International Offshore and Polar Engineering Conference (ISOPE 1995): The Hague, The Netherlands, June, 1995* [online]. ISOPE: OnePetro, 1995. No. ISOPE-I-95-013. [Accessed: June 2022]. Available at: <https://onepetro.org/ISOPEIOPEC/proceedings-abstract/ISOPE95/All-ISOPE95/ISOPE-I-95-013/2286 3>.

Viselli, A. M.; Goupee, A. J.; Dagher, H. J. Model test of a 1:8-scale floating wind turbine offshore in the Gulf of Maine. *Journal of Offshore Mechanics and Arctic Engineering* [online]. ASME, 2015, vol. 137, no. 4. p.041901. eISSN 1528-896X.[Accessed: June 2022]. Available at: <.https://doi.org/10.1115/1.4030381>.

Vugts, J. H. Comparing ringing loads from experiments with cylinders of different diameters : an empirical study. In: *Conference: BOSS `97: 8. international conference on the behaviour of offshore structures, Delft (Netherlands), 7-10 Jul 1997*. Delft: Delft Univ. of Technology, 1997. p. 95-112. ISBN 008042832.

Vyzikas, T.; Stagonas, D.; Buldakov, E.; Greaves, D. The evolution of free and bound waves during dispersive focusing in a numerical and physical flume. *Coastal Engineering* [online]. Elsevier, 2018, vol. 132, p. 95–109. eISSN 0378-3839. [Accessed: June 2022]. Available at: <https://doi.org/10.1016/J.COASTALENG.2017.11.003>.